# A Simple Active and Reactive Power Control for Applications of Single-Phase Electric Springs

Qingsong Wang, *Senior Member*, *IEEE*, Ming Cheng, *Fellow, IEEE*, Yunlei Jiang, *Student Member*, *IEEE*, Wujian Zuo, Giuseppe Buja, *Life Fellow*, *IEEE*

***Abstract*—Aiming at effective power management in microgrids with high penetration of renewable energy sources (RESs), the paper proposes a simple power control for the so-called second-generation, single-phase electric springs (ES-2), that overcomes the shortcomings of the existing ES control methods. By the proposed control, the unpredictable power generated from RESs is divided into two parts, i.e. the one absorbed by the ES-2 that still varies and the other injected into the grid that turns to be controllable, by a simple and accurate signal manipulation that works both at steady-state and during RES transients. It is believed that such a control is suitable for the distributed power generation, especially at domestic homes.**

**In the paper, the proposed control is supported by a theoretical background. Its effectiveness is at first validated by simulations and then by experiments. To this purpose, a typical RES application is considered, and an experimental setup is arranged, built up around an ES-2 implementing the proposed control. Testing of the setup is carried out in three steps and proves not only the smooth operation of the ES-2 itself, but also its capability in running the application properly.**

***Index Terms*—Electric spring, smart load, microgrids, power control, grid connected, distributed generation.**

## I. INTRODUCTION

CENTRALIZED control is adopted in the existing power system where power generation mainly depends on the load prediction. Nowadays, with the increasing portion of power generated from the renewable energy sources (RESs) and injected into the power system, stability issues become more and more severe due to the RES intermittency [1]. Flexible alternating current transmission systems are used to control voltage and/or power flow [2]–[5]. However, most of them are suitable for high- or medium-voltage applications, and cannot be used for future low-voltage microgrids with high RES penetration, such as roof photovoltaic (PV) and small power-rating wind plants [6]. To cope with this need, the electric spring (ES) technology has been proposed for future distributed microgrids [7] to transfer the line voltage fluctuations to the so-called non-critical loads (NCLs) [8], i.e. to the loads that tolerate a large supply voltage range, so as to keep regulated the voltage across the so-called critical loads (CLs), i.e. the loads that tolerate a narrow supply voltage range. The transfer occurs through an automatic balance of the load demand with the power generation, performed by ES. The set made of ES and NCLs forms the so-called smart load (SL). The voltage across CLs and the in-parallel SL is hereafter designated with grid voltage.

So far, many papers have appeared reporting on ES topologies [8]–[11] and their control strategies [12]–[16]. The first version (ES-1) in [8] can only manage the reactive power whilst the second version (ES-2) in [9] can manage both the active and the reactive power as the capacitor in the DC side of ES is replaced by a voltage source like a battery pack. The third version (ES-3) in [10] is a new type of ES without NCL. The so-sequenced fourth version (ES-4) in [11] changes the performance of ES greatly, since it compels the NCL voltage to vary in the same manner as the line voltage by the help of the insertion of an additional transformer in the original ES-2.

Previous works have reported various control schemes of the ES-2 [13]–[15]. For instance, [13] proposes the control of the input current by resorting to the *dq*0-transformation. This solution, however, is unable to keep unaltered the grid voltage as it is regulated in an open-loop mode. Even if a closed-loop with a proportional integral (PI) regulator is added to regulate the grid voltage, it mainly takes care of the power factor correction rather than of the voltage regulation. In [14], the $\delta$ control is proposed to adjust the instantaneous phase of CL voltage but relies on system modeling that utilizes the circuitry parameters. Recently, the radial-chordal decomposition (RCD) control is proposed in [15] to decouple the control of the power angle of SL from the voltage across CL, which makes ES-2 ready to be embedded in many devices such as water heaters. However, it still has some shortcomings. For instance, the

Manuscript received July26, 2017; revised September21, 2017 and December 4, 2017; accepted December20, 2017. This work was supported by the National Natural Science Foundation of China under project 51320105002 and the Natural Science Foundation of Jiangsu Province under project BK20170675. (*Corresponding author: Ming Cheng*)

Q. Wang, M. Cheng, Y. Jiang and W. Zuo are with the School of Electrical Engineering, Southeast University, Nanjing 210096, China. (e-mail: qswang@seu.edu.cn, mcheng@seu.edu.cn, yljiang1992@163.com, 220162254@seu.edu.cn)

G. Buja is with the Department of Industrial Engineering, University of Padova, Padova 35131, Italy. (giuseppe.buja@unipd.it)

This article has been accepted for publication in a future issue of this journal, but has not been fully edited. Content may change prior to final publication. Citation information: DOI 10.1109/TIE.2018.2793201, IEEE Transactions on Industrial Electronics



power angle of NCL should be known in advance, which prevents the use of the RCD control when NCL varies or is non-linear. Besides, it is difficult to obtain pure reactive power compensation by means of ES.

Power control of ES-2 is studied in this paper with reference to a practical application. Let us consider a low power outdoor wind power plant as an example The maximum power point tracking (MPPT) technique is normally adopted in the wind and/or solar power generation plants [17]–[18]. The tracked active power is consumed by the electrical loads at domestic homes, which are of both CL and NCL types. For an ES installed at the same location as the wind power plant, the active and reactive powers generated by the plant can be measured by ES even if they are changing quickly. As a result, ES in such situation can carry out the control of both the input active and reactive power and, by the latter control, can regulate the RMS value of the CL voltage at the pre-set value. For instance, the control scheme in [13] cannot handle the active power independently of the reactive one. Although constant active power compensation can be achieved by the $\delta$ control in [14], its shortcomings cannot still be overcome. Instead, the RCD control in [15] can regulate the grid voltage and can also correct the power factor of SL by the independent radial and chordal actions. However, [15] does not discuss the situation in which the input active power is constant. Even if one can demonstrate that the RCD control can deal with such a situation, calculations necessary to determine the reactive power that ES must provide are very involved, especially during the transients.

Aiming at the massive applications of ES-2 in the distributed power systems, this paper proposes a simple active and reactive power control as a solution to the shortcomings of the existing control methods. The proposed control not only decouples the active and reactive powers, but also relies on a local signal manipulation that does not need any information on the ES-2 circuitry parameters and the line voltage and parameters. Besides simulations, experiments are accomplished in three steps to verify the power management capabilities of the ES-2 implementing the proposed control.

In detail, this paper is organized as follows. Section II reviews the working principle of the ES-2 operated with the existing power control. Section III introduces the proposed power control and explains how it works. Section IV presents the simulations carried out on an ES-2 operated with the proposed control and discusses the simulation results. Section V gives experimental results obtained from a setup that consists of an ES-2 implementing the proposed control and a typical RES application. Finally, Section VI concludes the paper.

## II. Operating Principles of ES-2

### A. ES-2 Topology

As explained in [8], electric loads are divided into two types, namely CLs and NCLs. ES is an electrical device that is able to regulate the CL voltage at a pre-set value while passing the voltage (and power) fluctuations from the sources to NCL.

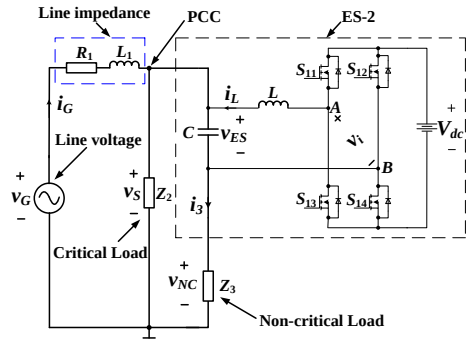


Fig. 1 Topology of ES-2 and associated circuitry.

The topology of ES-2 and the associated circuitry are drawn in Fig.1. In this figure, ES-2 is enclosed by the dashed line and consists of a single-phase voltage source inverter (VSI), an L filter and a capacitor whose voltage sums up to that of the NCL. Moreover, $Z_2$ is the CL, $Z_3$ is the NCL, $v_G$ represents the line voltage of the power system with RESs, $R_1$ and $L_1$ are the line resistance and inductance, respectively. The branch including $v_G$ and the line impedance supplies CL and SL. $v_S$ denotes the voltage of point of common coupling (PCC), which is also the CL voltage.

### B. Power Control of Existing ES-2

$\delta$ control is one of the power control methods for ES-2; its diagram is drawn in Fig. 2(a) and includes a double loop control. The outer loop is closed around the CL voltage by means of a PR regulator whilst the inner one is closed around the ES current by means of a P regulator.

The purpose of $\delta$ control is to set the instantaneous phase of the reference voltage for the PR regulator. The process of $\delta$ calculation is based on a vector analysis and ensures that ES operates at constant input active power mode [14]. Once the CL voltage is regulated, the control objectives of ES-2 are achieved. The $\delta$ calculation, which is executed by the blocks enclosed by the dashed line of Fig. 2(a), is the key element that affects operation of ES-2 and, hence, the fulfillment of the control objectives directly. However, $\delta$ calculation is based on a model of the ES-2 topology, shown in Fig. 1, and utilizes the parameters of the circuitry, thus impairing the control accuracy as they vary. What's more, as $\delta$ control is a phase control based on a vector diagram, it requires the RMS value of $v_G$ (marked as $V_G$) to calculate the angle $\delta$. Consequently, $V_G$ should be known in advance. In order to detect $V_G$, communication technique is needed between two neighboring ESs because $v_G$ is far away from ES-2 due to the transmission line between the ES-2 and the grid. This drawback leads to cost up when applying $\delta$ control to ES-2.

The RCD control diagram for ES-2 is drawn in Fig. 2(b). The ES voltage is here decomposed into two directions, named the radial and chordal ones. The PCC voltage is regulated by adjusting the apparent power absorbed by SL using the radial control whilst the power angle of SL is regulated at the pre-set value by the chordal control. This feature makes the SL smart as it allows ES-2 to achieve independent control of the apparent power and the power angle of SL. From this perspective, it follows that the RCD control aims at the power control of SL.

This article has been accepted for publication in a future issue of this journal, but has not been fully edited. Content may change prior to final publication. Citation information: DOI 10.1109/TIE.2018.2793201, IEEE Transactions on Industrial Electronics



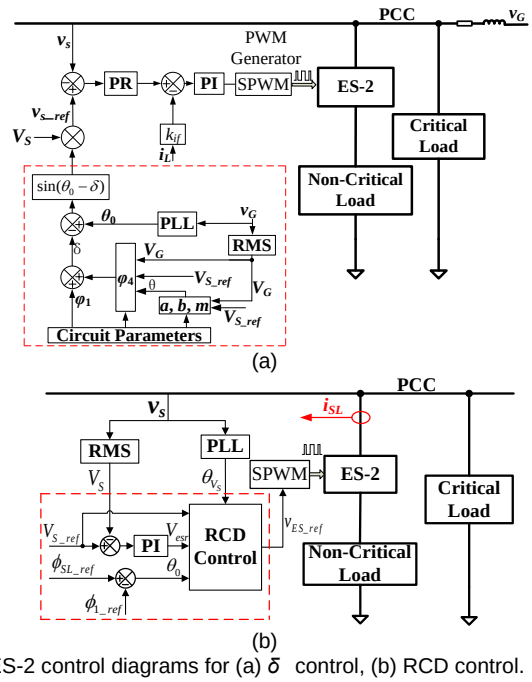


Fig. 2 ES-2 control diagrams for (a) $\delta$ control, (b) RCD control.

Although it is not like the $\delta$ control that needs almost all the circuitry parameters, impedance angle of NCL must be known in advance. It is also very difficult to operate ES-2 at pure reactive power compensation mode. Besides, how to deal with the situation when input active power is varying is not explained in [15].

### C. Requirements for the Proposed Power Control

Further to the analysis above, it would be desirable to dispose of a new power control method with the following requirements:

- No need to detect the information of grid voltage which is a far away from PCC, like $\delta$ control
- Need to decouple the control loop of the input active power from that of the PCC voltage or of the input reactive power
- Easy to implement and less computational burden compared to other techniques

## III. The Proposed Power Control

In this section, the proposed power control is presented, explaining its ability to achieve a simple active and reactive power control for ES-2 by a local signal manipulation. In the proposed control, the single-phase *dq* rotating frame is adopted.

### A. Active and Reactive Power of ES System

The sinusoidal voltage $v_S$(t) and current $i_1$(t) can be expressed as

$$v_S(t) = \sqrt{2}V_S \cos(\omega t + \phi) \tag{1}$$

$$i_1(t) = \sqrt{2}I_1 \cos(\omega t + \psi) \tag{2}$$

where $\phi$ and $\psi$ are the initial phases, $\omega$ is the angular frequency, $V_S$ and $I_1$ denote the rms value of $v_S$(t) and $i_1$(t), respectively.

By looking from PCC to the right side in Fig. 1, active, reactive and apparent powers can be expressed from (3) to (5), where $P_{in}$ and $Q_{in}$ are the total active and reactive power absorbed by ES, CL and NCL together, respectively; $\tilde{S}$ denotes the apparent power; $\vec{V}_S$ is the vector form of $v_S$(t); $\vec{I}_1^*$ is the conjugate vector form of $i_1$(t).

$$\begin{aligned}\tilde{S} &= \vec{V}_S \cdot \vec{I}_1^* \\ &= V_S I_1[\cos(\phi-\psi) + j\sin(\phi-\psi)] \\ &= P_{in} + jQ_{in}\end{aligned} \tag{3}$$

where

$$P_{in} = V_S I_1 \cos(\phi-\psi) \tag{4}$$

$$Q_{in} = V_S I_1 \sin(\phi-\psi) \tag{5}$$

According to [19], the active and reactive powers can be represented in terms of the variables on a rotating frame as

$$P_{in} = v_d i_d + v_q i_q \tag{6}$$

$$Q_{in} = v_q i_d - v_d i_q \tag{7}$$

where $v_d$ and $v_q$ are the components of $v_S$ in the *dq* rotating frame. The same analogy applies to $i_d$ and $i_q$.

If the voltage vector of $v_S$ is aligned along the *d*-axis of the rotating frame, (6) and (7) can be rewritten as

$$P_{in} = v_d i_d \tag{8}$$

$$Q_{in} = -v_d i_q \tag{9}$$

It should be remarked that (6) to (9) are used to explain the minus sign of the power control loops. It can be seen from (8) and (9) that the polarities of $P_{in}$ and $Q_{in}$ are different. By [19], $Q_{inref}$ should be entered on the minus side and $P_{inref}$ on the plus side. However, the input current in Fig. 3(a) is selected to have a direction opposite to that of grid-connected converter (GCC) in [19]. As a result, the positions of the active and reactive powers, and the relevant references are exchanged in Fig. 3(a) with respect to [19]. This is due to the direction chosen for the input current in Fig. 3(a).

The calculation of $P_{in}$ and $Q_{in}$ is detailed in Fig. 3(b), where the Fourier Transforms are used to extract the peak values and the phase angles from the detected quantities of $v_S$ and $i_1$. One can readily recognize that (4) and (5) underlie the diagram of Fig. 3(b).

The matrix for the transformation of a vector from the $\alpha\beta$ stationary frame to a *dq* rotating frame and its inverse are expressed as

$$T(\hat{\theta}) = \begin{bmatrix} \cos\hat{\theta} & \sin\hat{\theta} \\ -\sin\hat{\theta} & \cos\hat{\theta} \end{bmatrix} \tag{10}$$

$$T(\hat{\theta})^{-1} = \begin{bmatrix} \cos\hat{\theta} & -\sin\hat{\theta} \\ \sin\hat{\theta} & \cos\hat{\theta} \end{bmatrix} \tag{11}$$

where $\hat{\theta}$ is the instantaneous phase of the PCC voltage detected by a phase locked loop (PLL) block.

### B. Power Control of ES-2

The control diagram of the proposed simple power control is shown in the block of Fig. 3(a) enclosed by the dashed line. The control calls for the detection of variables such as the input current $i_1$ and the CL voltage $v_S$. The input active and reactive powers of the ES system, marked as $P_{in}$ and $Q_{in}$, are obtained by

manipulating the instantaneous values of $v_S$ and $i_1$ as illustrated by the scheme of Fig. 3(b), of which the function block already exists in the Matlab/Simulink.

According to Fig. 3(a), the RMS value and the instantaneous phase of the CL voltage are detected by the RMS and PLL blocks, respectively. The powers $P_{in}$ and $Q_{in}$ are controlled by separate PI regulators. Specifically, the regulator in the *d*-axis controls $P_{in}$ and that one in the *q*-axis controls $Q_{in}$. Alternatively, if the control objective is the CL voltage instead of $Q_{in}$, a loop outer the *q*-axis is added closed with a PI regulator, and its output represents the reference for $Q_{in}$, designated as $Q_{inref}$.

The output signals of the PI regulators in both the loops are processed through the inverse *dq*-to-*αβ* transformation to get the modulation signal $v_{comp1}$. It should be noticed that functionality of harmonic suppression is added in Fig. 3(a) by subtracting the harmonic component denoted as $v_{S\_h}$ from $v_{comp1}$. The drive signals for the VSI transistors are obtained by the SPWM technique, just after a limiter.

### C. Single-Phase PLL

The traditional Synchronous Reference Frame PLL (SRF-PLL) [20] is utilized to estimate the phase $\theta$ and the angular frequency $\omega$ of $v_S$. The diagram of the SRF-PLL is detailed in Fig. 3(c), where the estimated values of $\theta$ and $\omega$ are marked as $\hat{\theta}$ and $\hat{\omega}$, respectively. And $\omega^*$ denotes $100\pi$.

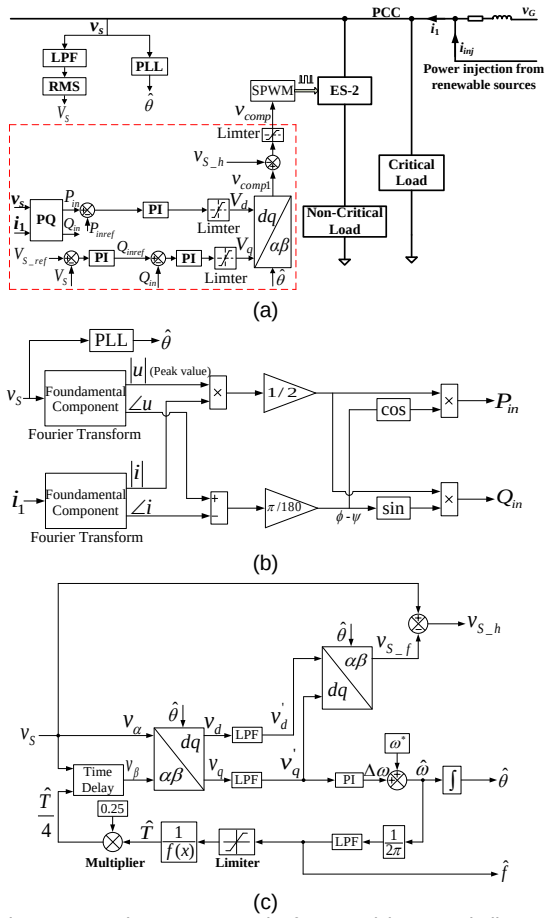


Fig. 3 The proposed power control of ES-2. (a) Control diagram. (b) Calculation diagram of active and reactive power. (c) Functions of PLL and harmonic extraction.

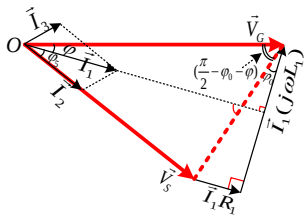

Fig. 4 Vector diagram of ES-2 circuit with resistive CL.

### D. Operating Limitations

ES-2 is believed to be able of controlling the input active power and the CL voltage independently. However, this is possible within certain limitations. The vector diagram in Fig. 4 is useful for further illustration, setting a resistive CL as an example. In Fig. 4, $\vec{I}_1$, $\vec{I}_2$, $\vec{I}_3$, $\vec{V}_G$, $\vec{V}_S$ represent the vectors of input, CL and NCL currents, and line and CL voltages, respectively. Angle $\varphi$ is defined as the phase angle by which $\vec{I}_1$ lags $\vec{V}_G$, $\varphi_5$ denotes the phase angle by which $\vec{I}_2$ lags $\vec{I}_1$, and $\varphi_0$ is the angle of line impedance. It can be deduced from (3) to (5) that once $V_G$ is fixed, a constant value of $P_{grid}$ implies that $I_1\cos\varphi$ is also constant, being $P_{grid}$ the active power generated by $v_G$. From [14] and Fig. 4, it derives that

$$\sin(\varphi+\varphi_5)=\frac{P_{grid}}{V_G V_S}\frac{\cos(\varphi+\varphi_0)}{\cos\varphi}\sqrt{R_1^2+(\omega L_1)^2} \quad (12)$$

The amplitude of the sin function is not greater than 1. Then, from (12), one gets

$$P_{grid}\le\left|\frac{V_G V_S}{\sqrt{R_1^2+(\omega L_1)^2}}\frac{\cos\varphi}{\cos(\varphi+\varphi_0)}\right| \quad (13)$$

By taking into account the fact that the line impedance of the microgrids is inductive, it follows that $\varphi_0$ is much less than $\varphi$, and the cosine terms in (13) can be ignored. Therefore, the maximum $P_{grid}$ can be approximated as

$$P_{grid}\le\frac{V_G V_S}{\sqrt{R_1^2+(\omega L_1)^2}} \quad (14)$$

Since $P_{grid}$ contains the losses of the transmission line, $P_{in}$ is less than $P_{grid}$.

## IV. Simulations and Discussions

To verify the aforementioned analysis, simulations are conducted using Matlab/Simulink based on parameters shown in Table I.

TABLE I
PARAMETERS FOR SIMULATION

| Items | Values |
|---|---|
| Regulated PCC voltage ($V_S$) | 220V |
| DC bus voltage ($V_{dc}$) | 400V |
| Line resistance ($R_1$) | 0.1Ω |
| Line inductance ($L_1$) | 2.4mH |
| Critical load ($R_2$) | 43.5Ω |
| Non-critical load ($R_3$) | 2.2Ω |
| Inductance of low-pass filter ($L$) | 3mH |
| Capacitance of low-pass filter ($C$) | 50μF |
| Switching frequency ($f_s$) | 20kHz |

To simplify the analysis, both CL and NCL are chosen of resistive types. It should be noticed that they can be any other linear types. For the ES-2 system under simulation, the control objectives are formulated as follows: i) RMS value of the PCC voltage or input reactive power is regulated at a pre-set values, and ii) input active power $P_{in}$ tracks the pre-set value $P_{inref}$.

Three situations are investigated, namely

- $P_{inref}$ varies at fixed $V_G$
- $V_G$ varies at fixed $P_{inref}$
- Distorted $V_G$

### A. Input Active Power Variation

In this part, three different values are selected for $V_G$ to monitor its behavior when $P_{inref}$ varies. Fig. 5 shows the simulation results when $P_{inref}$ varies. In each subfigure, four channels are recorded, reporting $v_G$, $P_{inref}$, $P_{in}$ and RMS value of the CL voltage, respectively.

Results in a full time range are also shown in Fig. 5(a), in which $P_{inref}$ is changed from 1.6kW to 1.1kW at 0.4s and then back to 1.6kW at 0.8s. It is observed that $P_{in}$ tracks $P_{inref}$ well while $V_S$ is regulated to 220V as $P_{inref}$ varies. To validate the proposed control further, the values of $P_{inref}$ are raised and simulated, as shown in Fig. 5(b). The waveforms confirm that the control objectives are also realized at high power ratings.

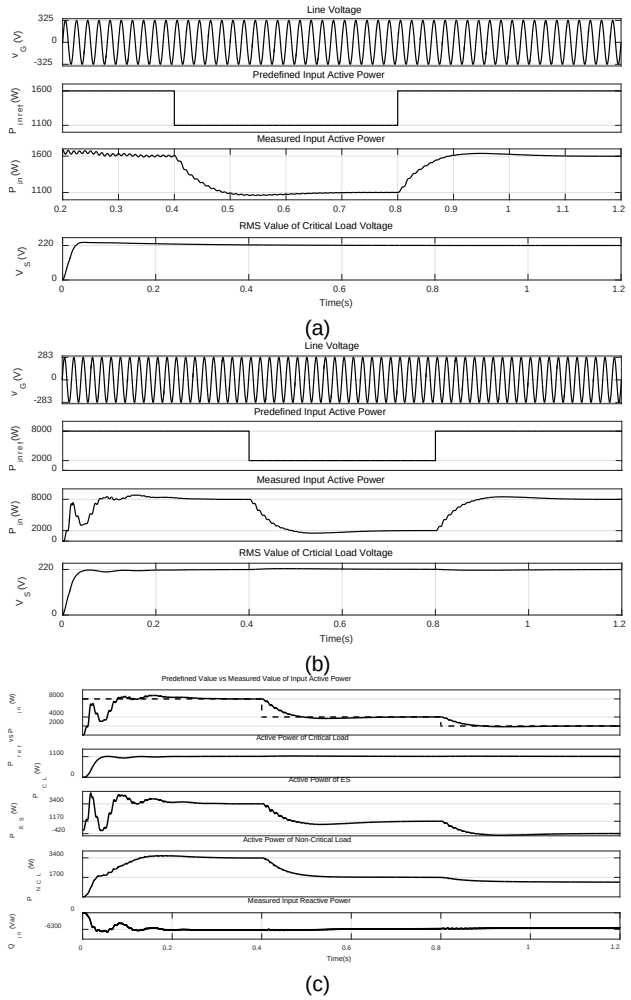


Fig. 5 Simulation waveforms under different variations of the input active power. (a) From 1.6kW to 1.1kW and then back to 1.6kW @ $V_G$=230V. (b) From 8kW to 2kW and then back to 8kW @ $V_G$=200V. (c) From 8kW to 4kW and then to 2kW @ $V_G$=200V.

To demonstrate how the control operates with the ES-2 power quantities, they are traced in Fig. 5(c), setting $V_G$=200 as an example. In each subfigure, four channels are recorded, reporting $P_{in}$, $P_{CL}$, $P_{ES}$ and $P_{NCL}$ against their pre-set values. The four power quantities represent the input active power, and the active powers absorbed respectively by the CL, the ES-2, and the NCL. In the first channel of each subfigure, $P_{inref}$ and $P_{in}$ are traced with the dashed and solid lines, respectively. In Fig. 5(c), $P_{inref}$ is set to 8kW from 0 to 0.4s, then to 4kW from 0.4s to 0.8s and then to 2kW from 0.8 to 1.2s. The results show that $P_{in}$ takes its reference at steady state. The active power of CL is almost regulated to 1kW during all the simulation time. When $P_{inref}$ is set to 8kW, the active powers of ES-2 and NCL are around 3.4kW and 3.4kW, respectively, which means that ES-2 is absorbing active power. However, when $P_{inref}$ drops to 2kW, the active powers of ES and NCL are around -420W and 1.31kW, which means that ES-2 is providing active power. The results also reveal that active powers of both ES and NCL vary in the same way as that of $P_{in}$. Therefore, ES not only acts as a power manager that passes the power fluctuations from input voltage sources to NCL, but also acts as an energy storage device that absorbs and/or provides powers.

### B. Line Voltage Variation

In this Subsection, the ES-2 transient responses to a change of $V_G$ are monitored with $P_{inref}$ fixed. They are traced in Figs. 6 (a) and (b). In each subfigure, four channels are recorded, reporting line voltage, reference value of the input active power, input active power and RMS value of CL voltage, respectively.

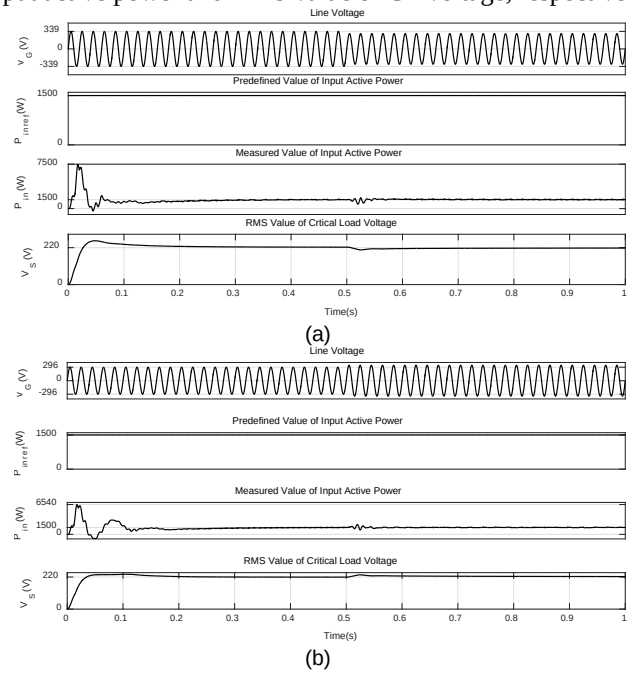


Fig. 6 Transient ES-2 responses to a change of the line voltage with $P_{inref}$=1.5kW. (a) From 240V to 210V. (b) From 210V to 240V.

In Fig. 6(a), $V_G$ is changed between two different values, more specifically it is equal to 240V from 0 to 0.5s; afterwards,

it jumps to 210V at 0.5s and remains at this value up to 1s. The change of $V_G$ in Fig. 6(b) is the opposite of that in Fig. 6(a). In both the simulations, $P_{inref}$ is set to 1.5kW and $P_{in}$ remains at the pre-set value very accurately. Meanwhile, the RMS value of the CL voltage is regulated to 220V as required.

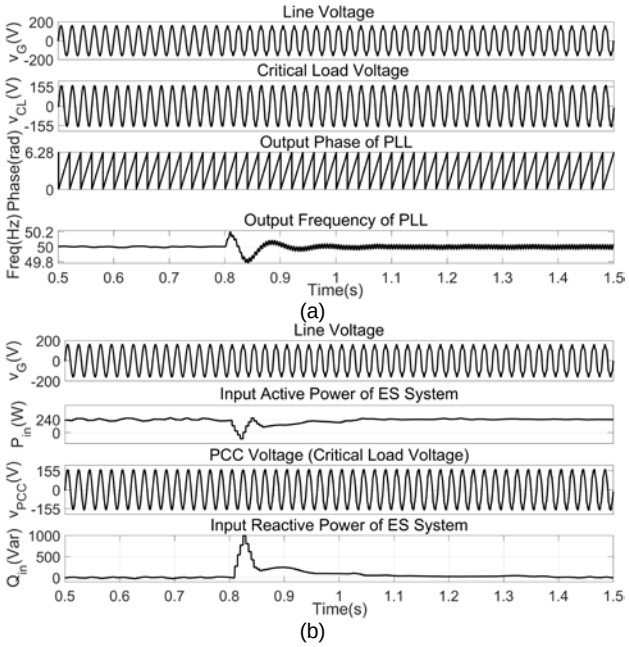


Fig. 7 Simulation waveforms before and after grid distortion. (a) Results of PLL. (b) Results of active and reactive power of ES system.

### C. Grid Distortion

In this part, performances of the ES system under grid distortion are observed. Besides, the waveforms of PLL are also provided, as shown in Fig. 7.

In Fig. 7(a), four channels are recorded as line voltage, CL voltage which is also PCC voltage, output phase of PLL, and output frequency of PLL, respectively. From 0.5 to 0.8s, $V_G$ is 110V without any distortion. However, from 0.8s to 1.5s, $V_G$ is added with the 3rd and 5th harmonic components, each 11V, respectively. It is seen that the output phase of PLL are stable during the simulation time even there is distortion on the line voltage. Before 0.8s, the output frequency is stable at 50Hz. Although fluctuations are seen in the output frequency in the fourth channel from 0.8s to 1.5s, the fluctuating range is only from 49.97Hz to 50.03Hz. Fig. 7(b) shows that the input active and reactive powers of ES system are also regulated well to follow the predefined values under the condition of grid distortion.

### D. Discussions

The essence of a power control of the ES-2, can be summarized as follows. It can achieve only two objectives, namely i) the regulation of the CL voltage by acting on the input reactive power, and ii) the control of the phase angle between voltage and current of the ES-2 by acting on the input active power.

Regarding $\delta$ control in [14], the key objective is the regulation of the CL voltage. All the compensation modes are related to the control of the phase angle between voltage and current of the ES-2. For instance, such phase angle should be precisely 90° at pure reactive power compensation mode. For constant input active power control mode, the phase angle will no longer be 90°, but varies with the input active power. The same applies to the other compensation modes. From this point of view, the proposed control can cover all the cases of $\delta$ control by changing the upper loop in Fig. 3(a), not to mention that it gets rid of the circuitry parameters. The essence of the RCD control is to control both the CL voltage and the power angle of the SL. According to the analysis above, such control is encompassed by the proposed control if only just the upper loop in Fig. 3(a) is used to adjust the power angle of the SL.

To summarize, it emerges that, besides an easy implementation, the key advantage of the proposed control is that it works irrespectively of the circuitry parameters.

## V. Application and Experiments

To double check the effectiveness of the proposed control, a feasibility study has been carried out in the laboratory, by coupling the ES-2 to an application as depicted in Fig. 8(a). This is obtained by adding a GCC block to the diagram in Fig. 1 with the purpose of emulating the power generation from the RES. The DC side of the GCC is supplied by a DC voltage source. In Fig. 8(a), $v_G$ is obtained from the grid through a variac. $Z_1$ emulates the line impedance between PCC and $v_G$. $Z_C$ is connected to PCC directly.

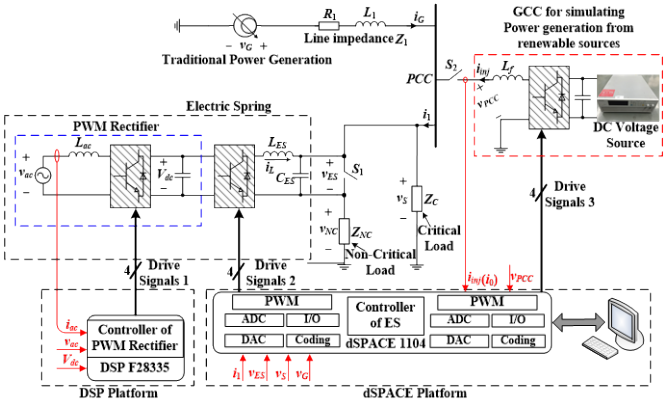


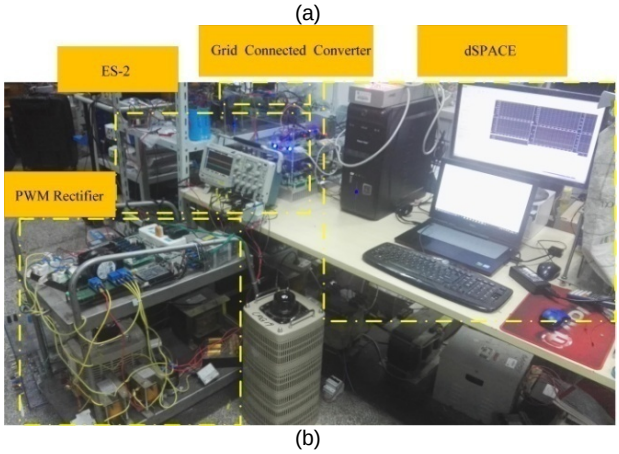


Fig. 8 Application and setup of experiments. (a) Diagram of implementation. (b) Picture of experimental setup.

This article has been accepted for publication in a future issue of this journal, but has not been fully edited. Content may change prior to final publication. Citation information: DOI 10.1109/TIE.2018.2793201, IEEE Transactions on Industrial Electronics



The setup includes two enable switches, one is designated as $S_1$ and is placed in parallel with the capacitor of the ES-2, and the other one is designated as $S_2$ and is placed in series with the GCC. The picture of experimental setup is shown in Fig. 8(b). The ES is deactivated by switching on $S_1$ since it shortens the capacitor and connects the NCL at PCC. If $S_2$ is off, the GCC is detached from PCC. The DC side of the inverter within the ES-2 is supplied by a PWM rectifier, controlled by a digital signal processing (DSP) platform based on TMS320F28335. The ES-2 system and the GCC are controlled by the dSPACE 1104 platform.

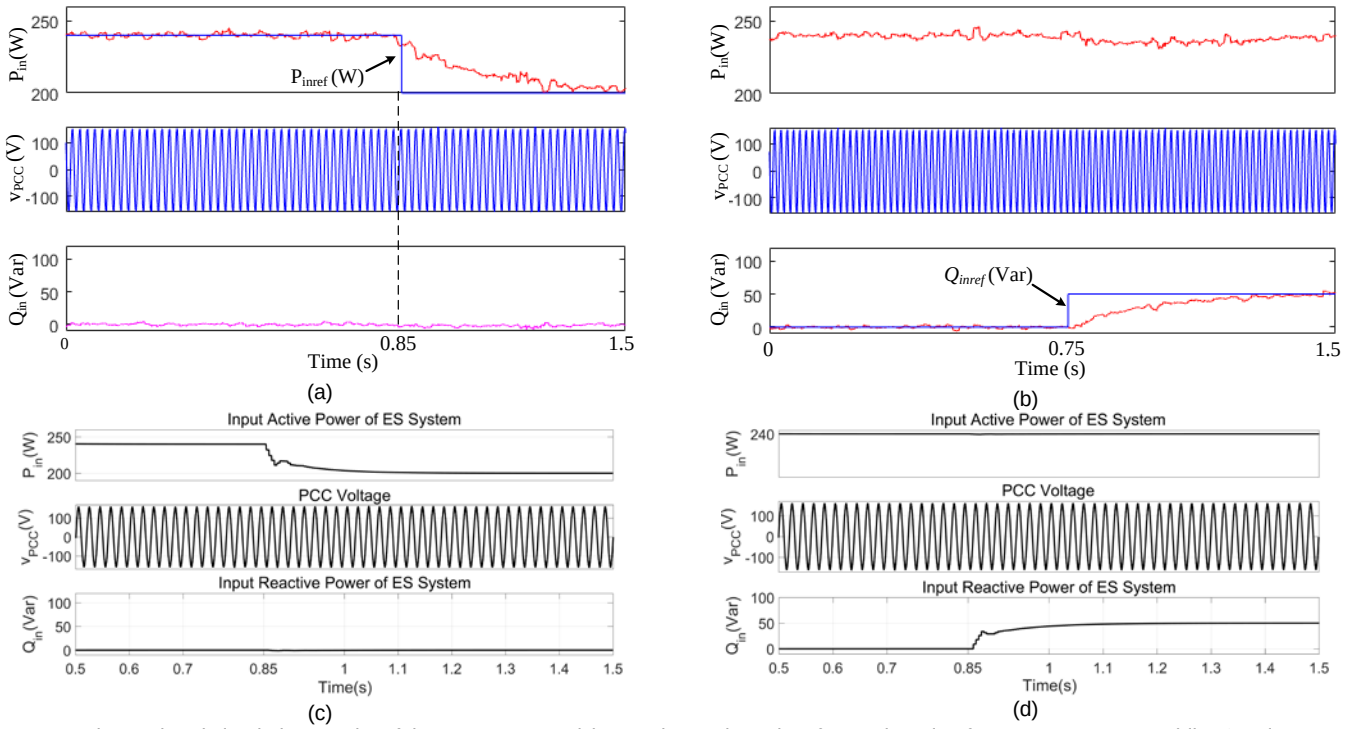


Fig. 9 Experimental and simulation results of the ES-2 system. (a) Experimental results of $P_{inref}$ changing from 240W to 200W whilst $Q_{inref}$ is set to 0. (b) Experimental results of $Q_{inref}$ changing from 0 to 50Var whilst $P_{inref}$ is set to 240W. (c) Simulation results of $P_{inref}$ changing from 240W to 200W whilst $Q_{inref}$ is set to 0. (d) Simulation results of $Q_{inref}$ changing from 0 to 50Var whilst $P_{inref}$ is set to 240W.

TABLE II
PARAMETERS FOR EXPERIMENTS

| Items | Values |
|---|---|
| Regulated PCC voltage ($V_S$) | 110V |
| DC bus voltage ($V_{dc}$) | 200V |
| Line resistance ($R_1$) | 0.1Ω |
| Line inductance ($L_1$) | 1.45mH |
| Critical load ($R_2$) | 2000Ω |
| Non-critical load ($R_3$) | 50Ω |
| Inductance of low-pass filter ($L$) | 3mH |
| Capacitance of low-pass filter ($C$) | 50μF |
| Inductance of filtering inductor ($L_f$) | 11.34mH |
| Switching frequency of the rectifier ($f_{rec}$) | 20kHz |
| Switching frequency of the GCC ($f_{GCC}$) | 10kHz |
| Switching frequency of the ES ($f_{ES}$) | 10kHz |

The experiments are executed in three steps. The first step is intended to verify the operation of the ES-2 when implementing the proposed control and is performed by switching off both $S_1$ and $S_2$. The second step is intended to check the behavior of the GCC in emulating the power injection from a RES and is performed by switching on both $S_1$ and $S_2$. The third step is intended to jointly debug both the ES-2 and the GCC to validate the effectiveness of the power control in a real application and is performed by switching $S_1$ off and $S_2$ on. Parameters of the experimental setup are listed in Table II.

### A. *Only the ES-2 is Activated (Step 1)*

In this Subsection, both $S_1$ and $S_2$ are turned off, which means that the ES-2 is activated and the GCC is detached. The experimental waveforms obtained from the ES-2 system are shown in Figs. 9 (a) and (b), where three channels are recorded, reporting $P_{inref}$ versus $P_{in}$, the CL voltage $v_S$ which is also PCC voltage and the input reactive power $Q_{in}$. As mentioned previously, $P_{in}$ is the total active power absorbed by the CL, the NCL and the ES-2. In Fig. 9(a), $Q_{inref}$ is set to 0 whilst $P_{inref}$ is set to 240W from 0 to 0.85s and to 200W from 0.85s to 1.5s. It can be observed that $P_{in}$ and $Q_{in}$ track the references smoothly. In Fig. 9(b), $P_{inref}$ is set to 240W whilst $Q_{inref}$ is set to 0 before 0.75s and to 50Var from 0.75s to 1.5s. Before 0.75s, the mean value of $P_{in}$ is almost steady at 240W, ignoring the moderate fluctuations. After 0.75s, although decreasing a little just after the change of $Q_{inref}$, $P_{in}$ goes back to 240W finally. Moreover, the third channel of Fig. 9(b) shows that $Q_{in}$ settles at the required value of 50Var at steady state. Figs. 9 (a) and (b) confirm the deocupled power control ability of ES-2 with the proposed control. In order to increase the readability, simulation results are added in Figs. 9 (c) and (d), which are shown to compare with Figs. 9 (a) and (b), respectively.

This article has been accepted for publication in a future issue of this journal, but has not been fully edited. Content may change prior to final publication. Citation information: DOI 10.1109/TIE.2018.2793201, IEEE Transactions on Industrial Electronics



### *B. Only the GCC is Activated (Step 2)*

In this Subsection, both $S_1$ and $S_2$ are turned on to deactivate the ES and connect the GCC. The purpose is to check the behavior of the PCC voltage with different power injections. In order to distinguish the power in the different steps, the active and reactive power generated by the GCC are hereafter denoted with $P_{inj}$ and $Q_{inj}$, and the reference of $P_{inj}$ is denoted with $P_{injref}$. Besides, the current injected into PCC is termed as $I_0$.

The active and reactive power control is also used in the GCC. The experimental waveforms are shown in Fig. 10, where the quantities in the first three channels are the same as in Fig. 9. The only difference is an additional channel to monitor $I_0$ and the trace of PCC voltage is zoomed out by one fifth of its normal value.

In Fig. 10, the reference value of $Q_{inj}$ is set to zero, which means that only active power is injected into PCC. The results point out that the control of $P_{inj}$ works well as it keeps $P_{inj}$ tracking $P_{injref}$. Meanwhile, the current injected into PCC is controlled so as to be in phase with the PCC voltage also in the presence of a step variation of $P_{inj}$.

The reason why PCC voltage looks so stale with power injection is as follows. The intention of this part is to use GCC to simulate an intermittent power generated from RESs, which should be managed by the ES-2. In the distributed power system, a single power injection at one place has little influence due to its limited power rating. However, if many of such power generations inject power to the grid, the influence will be huge. The huge power injection to the grid could not be simulated in the laboratory due to limitation. As a result, such little active power injected by the GCC is so limited and has almost no influence on the PCC.

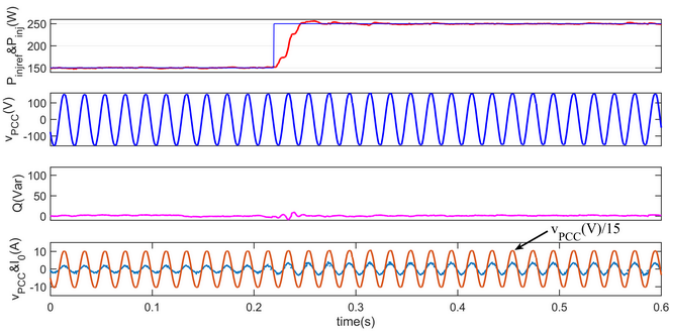


Fig. 10 Experimental waveforms when $P_{injref}$ steps from 150W to 250W whilst $Q_{injref}$ is set to 0.

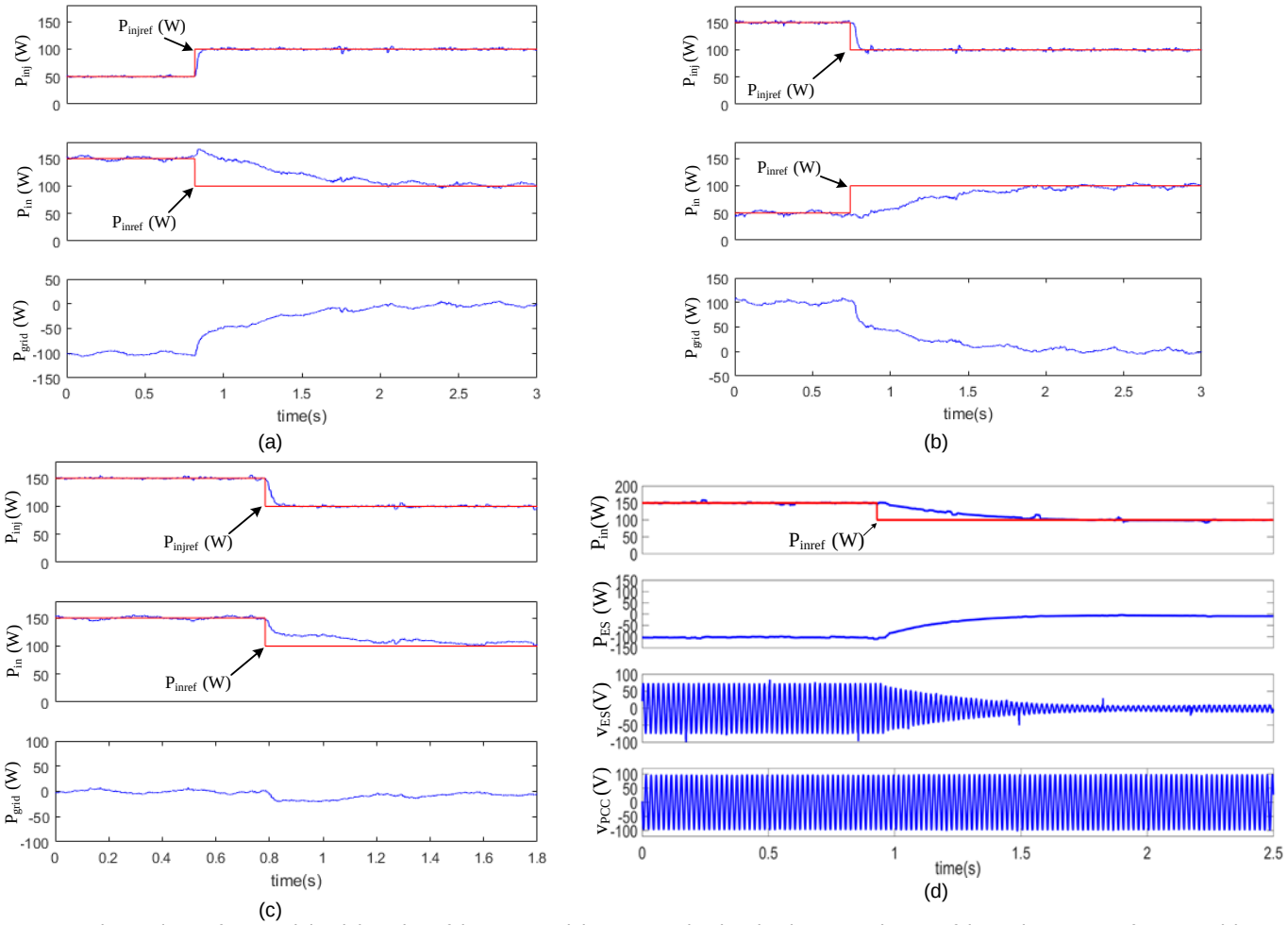


Fig. 11 Experimental waveforms at joint debugging of the ES-2 and the GCC under the simultaneous change of the active power references. (a) $P_{injref}$ changes from 50W to 100W and $P_{inref}$ changes from 150W to 100W. (b) $P_{injref}$ changes from 150W to 100W and $P_{inref}$ changes from 50W to 100W. (c) Both $P_{injref}$ and $P_{inref}$ change from 150W to 100W. (d) Waveforms of active power of ES-2 and voltages of ES and PCC when $P_{inref}$ changes from 150W to 100W.

### C. Joint Debug of the ES-2 and the GCC (Step 3)

In this Subsection, only $S_2$ is switched on so that both the ES-2 and the GCC are activated and the power control ability of the ES-2 in a real application is tested. There are many situations of power change; three of them, which take place typically in practice, are here presented. The relevant experimental waveforms are shown in Figs. 11 (a)-(d).

The measured quantities reported in the three channels of Figs. 11 (a)-(c) are active power generated by GCC, active power absorbed by the ES system, active power sent to the grid. In detail, $P_{injref}$ and $P_{inj}$ are given in the first channel whilst $P_{inref}$ and $P_{in}$ are given in the second channel. The power sent to grid is $P_{grid}$ which is given in the third channel.

In each situation, there is a step of the reference of active power. In Fig. 11(a), $P_{injref}$ and $P_{inref}$ are set initially to 50W and 150W, respectively, and then both are set to 100W.

The results outline that both $P_{inj}$ and $P_{in}$ track their references, although the response time of $P_{in}$ is more sluggish than that of $P_{inj}$. Initially, the GCC generates 50W whilst the CL, the NCL and the ES-2 absorb 150W; hence the grid has to generate 100W to meet the load demand. After the change of the power references, the active power generated by the GCC is almost completely absorbed by the ES-2 system. Consequently, the grid does not absorb or provide any active power.

In Fig. 11(b), initially the GCC generates 150W whilst the ES-2 system absorbs 50W, the rest power being sent to grid. The responses after the change of the power references are similar to those in Fig. 11(a). In Fig. 11(c), $P_{injref}$ and $P_{inref}$ are set to be equal both before and after the change. It appears from the traces that the grid does not absorb or provide any active power at steady state since $P_{inj}$ and $P_{in}$ remain nearly equal also after the power change. It can be deduced from the experimental results that, if the ES-2 and the GCC are located together, $P_{inj}$ is properly detected and managed by the ES-2 so that the power sent to grid turns to be controllable.

Fig. 11(d) is added to show the waveforms of the active power of ES-2, ES-2 voltage and PCC voltage when the input active power is changing. It is seen that when $P_{inref}$ changes from 150W to 100W, the PCC voltage and $P_{in}$ are controlled well. Meanwhile, the test result in channel 2 shows that the active power of ES also changes as $P_{in}$ changes. After 1s, when the input active power is low, the ES has to provide active power to make sure a stable power on the CL.

### D. Remarks of Parameter Tuning

It should be noted that the trial-and-error method was adopted during parameter tuning. The estimated controller bandwidth is about 40Hz. The $k_p$ and $k_i$ of both PI controllers in Fig. 3(a) are set to 0.0008 and 0.02, respectively.

## VI. Conclusion

The input active and reactive power control is proposed for the purpose of practical application of ES-2 in this paper. An overall review and analysis have been done on the existing control strategies such as $\delta$ control and RCD control, revealing that the essences of the controls on ES-2 are to control the input active power and reactive power. If being equipped together with the distributed generation from RESs, the ES-2 can manage the fluctuated power and make sure the controllable power to grid, which means that the ES-2 is able to deal with the active power captured by MPPT algorithm. Simulations have been done on the steady and transient analysis and also under the grid anomalies, validating the effectiveness of the proposed control. Three steps have been set in the experiments to verify the three typical situations and namely the active power generated by the GCC from RESs are, 1) more than; 2) less than; 3) the same as the load demand. Tested results have validated the proposed control.

## References


[1] M. Cheng and Y. Zhu, "The state of the art of wind energy conversion systems and technologies: Areview," *Energy Conversion and Management*, vol. 88, pp. 332–347, Dec. 2014.

[2] P. Sotoodeh and R. D. Miller, "Design and implementation of an 11-level inverter with FACTS capability for distributed energy systems," *IEEE J. Emerging Sel. Topics Power Electron.*, vol.2, no. 1, pp. 87–96, Mar. 2014.

[3] L. Wang, and D. N. Truong, "Stability enhancement of a power system with a PMSG-based and a DFIG-based offshore wind farm using a SVC With an adaptive-network-based fuzzy inference system," *IEEE Trans. Ind. Electron.*, vol. 60, no. 7, pp. 2799–2807, Jul. 2013.

[4] Y. Zhang, X. Wu and X. Yuan, "A simplified branch and bound approach for model predictive control of multilevel cascaded H-bridge STATCOM," *IEEE Trans. Ind. Electron.*, vol. 64, no. 10, pp. 7634–7644, Oct. 2017.

[5] W. Wang, L. Yan, X. Zeng, B. Fan, and J. M. Guerrero, "Principle and design of a single-phase inverter based grounding system for neutral-to-ground voltage compensation in distribution networks," *IEEE Trans. Ind. Electron.*, vol. 64, no. 2, pp. 1204–1213, Feb. 2017.

[6] Q. Sun, J. Zhou, J. M. Guerrero, and H. Zhang, "Hybrid three-phase/single-phase microgrid architecture with power management capabilities," *IEEE Trans. Power Electron.*, vol. 30, no. 10, pp. 5964–5977, Oct. 2015.

[7] J. M. Guerrero, J. C. Vasquez, J. Matas, L. G. de Vicuna, and M. Castilla, "Hierarchical control of droop-controlled AC and DC microgrids—a general approach toward standardization," *IEEE Trans. Ind. Electron.*, vol. 58, no. 1, pp. 158–172, Jan. 2011.

[8] S. Y. R. Hui, C. K. Lee, and F. Wu, "Electric springs—A new smart grid technology," *IEEE Trans. Smart Grid*, vol. 3, no. 3, pp. 1552–1561, Sept. 2012.

[9] S. C. Tan, C. K. Lee, and S. Y. R. Hui, "General steady-state analysis and control principle of electric springs with active and reactive power compensations," *IEEE Trans. Power Electron.*, vol. 28, no. 8, pp. 3958–3969, Aug. 2013.

[10] C. K. Lee and S. Y. R. Hui, "Input AC voltage control bi-directional power converters," U.S. Patent 13/907, 350, May 31, 2013.

[11] Q. Wang, M. Cheng, G. Buja, and Z. Chen, "A novel topology and its control of single-phase electric springs," in *Proc. Int. Conf. Renewable Energy Res. Appl.*, 2015, pp. 267–272.

[12] Q. Wang, M. Cheng, and Y. Jiang, "Harmonics suppression for critical loads using electric springs with current-source inverters," *IEEE J. Emerging Sel. Topics Power Electron.*, vol. 4, no. 4, pp. 1362–1369, Dec. 2016.

[13] S. Yan, S. C. Tan, C. K. Lee, and S. Y. R. Hui, "Electric spring for power quality improvement," in *Proc. IEEE Appl. Power Electron. Conf. Expo.*, 2014, pp. 2140–2147.

[14] Q. Wang, M. Cheng, Z. Chen, and Z. Wang, "Steady-state analysis of electric springs with a novel $\delta$ control," *IEEE Trans. Power Electron.*, vol. 30, no. 12, pp. 7159–7169, Dec. 2015.

[15] K. T. Mok, S. C. Tan, and S. Y. R. Hui, "Decoupled power angle and voltage control of electric springs," *IEEE Trans. Power Electron.*, vol. 31, no. 2, pp. 1216–1229, Feb. 2016.

[16] X. Chen, Y. Hou, S. C. Tan, C. K. Lee, and S. Y. R. Hui, "Mitigating voltage and frequency fluctuation in microgrids using electric springs," *IEEE Trans. Smart Grid*, vol. 6, no. 2, pp. 508–515, Mar. 2015.

[17] M. Andresen, G. Butichi, and M. Liserre, "Thermal stress analysis and MPPT optimization of photovoltaic systems," *IEEE Trans. Ind. Electron.*, vol. 63, no. 8, pp. 4889–4898, Aug. 2016.
[18] F. Paz, and M. Ordonez, "High-performance solar MPPT using switching ripple identification based on a lock-in amplifier," *IEEE Trans. Ind. Electron.*, vol. 63, no. 6, pp. 3595–3604, Jun. 2016.
[19] J. A. Munoz, J. R. Espinoza, C. R. Baier, L. A. Moran, E. E. Espinosa, P. E. Melin, and D. G. Sbarbaro, "Design of a discrete-time linear control strategy for a multicell UPQC," *IEEE Trans. Ind. Electron.*, vol. 59, no. 10, pp. 3797–3807, Oct. 2012.
[20] S. Golestan, and J. M. Guerrero, "Conventional synchronous reference frame phase-locked loop is an adaptive complex filter," *IEEE Trans. Ind. Electron.*, vol. 62, no. 3, pp. 1679–1682, Mar. 2015.

**Qingsong Wang** (S'14–M'17–SM'17) received the B.Sc. and M.Sc. degrees from the Department of Electrical Engineering, Zhejiang University, Hangzhou, China, in 2004 and 2007, respectively, conducting researches in multi-level current source converters, and the Ph.D. degree from the School of Electrical Engineering, Southeast University, Nanjing, China, in 2016. From November 2015 to November 2016, he was a joint Ph.D. student with the Department of Energy Technology, Aalborg University, Aalborg, Denmark, where he focused on the control of electric springs.

From July 2004 to July 2005, he was an engineer in Shihlin Electronic & Engineering Co., Ltd, Suzhou, China. From July 2007 to August 2011, he was an engineer in Global Development Center of Philips Lighting Electronics, Shanghai, China. In October 2010, he was promoted to be a Senior Engineer. From August 2011 to September 2013, he was a Lecturer in PLA University of Science and Technology, Nanjing, China. Since 2017, he has been with Southeast University, where he is currently a Lecturer in the School of Electrical Engineering.

Dr. Wang's research interests are focused in the areas of control and applications of power electronics to power systems, smart grid and lighting drivers.

**Ming Cheng** (M'01–SM'02–F'15) received the B.Sc. and M.Sc. degrees in Electrical Engineering from the Department of Electrical Engineering, Southeast University, Nanjing, China, in 1982 and 1987, respectively, and the Ph.D. degree from the Department of Electrical and Electronic Engineering, The University of Hong Kong, Hong Kong, in 2001, all in electrical engineering.

Since 1987, he has been with Southeast University, where he is currently a Chair Professor in the School of Electrical Engineering and the Director of the Research Center for Wind Power Generation. From January to April 2011, he was a Visiting Professor with the Wisconsin Electric Machine and Power Electronics Consortium, University of Wisconsin, Madison. His teaching and research interests include electrical machines, motor drives for electric vehicles, and renewable energy generation. He has authored or coauthored over 360 technical papers and 5 books and is the holder of 100 patents in these areas.

Prof. Cheng is a fellow of the Institution of Engineering and Technology. He has served as chair and organizing committee member for many international conferences. He is a Distinguished Lecturer of the IEEE Industry Applications Society (IAS) in 2015/2016.

**Yunlei Jiang** (S'14) received the B.Sc. degree in electrical engineering from Nanjing Normal University, China, in 2015. He is currently working towards the M.Sc. degree at the School of Electrical Engineering, Southeast University, Nanjing, where he focused on the control of brushless doubly fed generators for stand-alone and grid-connected applications.

His research interests are mainly on the analysis and control of brushless ac machines in wind energy conversion systems.

**Wujian Zuo** received the B.Sc. degree in the School of Electrical Engineering and Control Science from Nanjing Tech University, Nanjing, China, in 2016. He is currently working towards the M. Sc. degree in the School of Electrical Engineering at Southeast University, Nanjing, China, where he focused on the control of electric springs.

His current research interests include applications of power electronics to power systems.

**Giuseppe Buja** (M'75–SM'84–F'95–LF'13) received the "Laurea" degree with honors in power electronics engineering from the University of Padova, Padova, Italy, where he is currently a Full Professor.

He has carried out an extensive research work in the field of power and industrial electronics, originating the modulating-wave distortion and the optimum modulation for pulse-width modulation inverters, pioneering the introduction of digital signal processing in the control systems of power electronics converters, and conceiving advanced techniques for the control of electric drives. His current research interests are automotive electrification, including wireless charging of electric vehicles, and grid-integration of renewable energies.

Dr. Buja received the IEEE Industrial Electronics Society (IES) Eugene Mittelmann Achievement Award "in recognition of his outstanding technical contributions to the field of industrial electronics," and the 2016 Best Paper Award from the IEEE Transactions on Industrial Electronics. He has served the IEEE in several capacities, including as General Chairman of the 20th Annual Conference of the IES (IECON) in 1994. Currently, he is an Associate Editor of the IEEE Transactions on Industrial Electronics, a Member of the Editorial Board of the Chinese Journal of Electrical Engineering, and a Senior Member of the Administrative Committee of the IES.